Applied Catalysis B: Environmental 320 (2023) 121936

Contents lists available at ScienceDirect

Applied Catalysis B: Environmental

journal homepage: www.elsevier.com/locate/apcatb

On the role of Zr to facilitate the synthesis of diesel and jet fuel range intermediates from biomass-derived carbonyl compounds over aluminum phosphate

Wenting Fang [a], Sihang Liu [b], Leonhard Schill [a], Mariusz Kubus [a], Thomas Bligaard [c], Anders Riisager [a,*]

[a] Centre for Catalysis and Sustainable Chemistry, Department of Chemistry, Technical University of Denmark, DK-2800 Kgs. Lyngby, Denmark
[b] Catalysis Theory Center, Department of Physics, Technical University of Denmark, DK-2800 Kgs. Lyngby, Denmark
[c] Department of Energy Conversion and Storage, Technical University of Denmark, DK-2800 Kgs. Lyngby, Denmark

ARTICLE INFO

Keywords:
Aldol condensation
Biomass conversion
Zr-modified aluminum phosphate
Cyclohexanone
Furfural

ABSTRACT

Heterogeneous zeolite/zeotype catalysts are attractive for converting renewable biomass-derived chemicals into transportation fuels by aldol condensation reactions, which provide a simple strategy to improve carbon numbers. Herein, Zr-doped aluminum phosphate (ZrAPO-5) were applied for efficient syntheses of diesel and jet fuel range C_{11}, C_{12} and C_{16} intermediates from biomass-derived furfural (FF) and cyclohexanone (CH). Incorporation of Zr in the APO-5 framework facilitated the adsorption of the C═O groups of FF and CH and created more and stronger acid and base sites, which co-catalyzed the aldol condensation and facilitated the product yields. ZrAPO-5 (Zr/Al = 0.20) yielded up to 79.3% single aldol condensation product C_{11} or 80.7% double aldol condensation product C_{16} in the cross-aldol condensation of FF and CH under appropriate reaction conditions, and also realized 83.3% C_{12} yield in the self-aldol condensation of CH. In addition, the catalytic system displayed good to excellent yields of other value-added chemicals in aldol condensations of alternative carbonyl compounds.

1. Introduction

Catalytic conversion of renewable biomass to chemicals and potential fuels is a highly relevant topic for dealing with global challenges such as environmental preservation and the future energy demand.[1] Especially the synthesis of diesel and jet fuel range hydrocarbons from lignocellulose-derived platform compounds has drawn tremendous attention,[2,3] and one of the frequently adopted strategies to increase carbon numbers of biomass-derivatives for producing jet fuel (C_{9-14}) and diesel (C_{12-20}) is the aldol condensation of carbonyl compounds.[4] The reaction may occur between two ketones, two aldehydes or an aldehyde and a ketone.

Furfural (FF) and cyclohexanone (CH) are platform chemicals with carbonyl groups which may be derived from xylose and aromatic ethers [5,6] though CH synthesized from the biomass-derived compounds is not widely used. The cross-aldol condensation between FF and CH can generate (*E*)-2-(furan-2-ylmethylene)cyclohexan-1-one (labelled C_{11}) and (2*E*,6*E*)-2,6-bis(furan-2-ylmethylene)cyclohexan-1-one (labelled C_{16}).[7] The self-aldol condensation of CH forms two isomers, [1,1'-bi(cyclohexylidene)]-2-one and [1,1'-bi(cyclohexan)]-1'-en-2-one (together labelled C_{12}) (Scheme 1). All of the C_{11}, C_{12} and C_{16} compounds are fuel precursors with high volumetric energy density and high pour point.[7,8]

In order to generate C–C bonds with carbonyl compounds, bases are typically exploited for the abstraction of α-protons to form the enolate intermediate required for the bond formation.[9] Accordingly, homogeneous basic catalysts (e.g., NaOH and $Ca(OH)_2$) [10–12] and heterogeneous basic catalysts (e.g., earth alkali oxides, MgZr or MgAl mixed oxides and hydrotalcite) [13–16] have been widely used for the aldol condensation between FF and ketones. Although homogeneous basic catalysts show excellent activity and high selectivity for the desired products, several drawbacks remain during the synthesis, such as catalyst/product separation and equipment corrosion.[9] Heterogeneous basic catalysts could circumvent these issues and are thus preferred, however, they are easily deactivated in the presence of furoic acid which can form as byproduct by base-catalyzed Cannizzaro reaction of FF.[7,

* Corresponding author.
E-mail address: ar@kemi.dtu.dk (A. Riisager).

https://doi.org/10.1016/j.apcatb.2022.121936
Received 4 June 2022; Received in revised form 12 August 2022; Accepted 1 September 2022
Available online 5 September 2022
0926-3373/© 2022 The Author(s). Published by Elsevier B.V. This is an open access article under the CC BY license (http://creativecommons.org/licenses/by/4.0/).

17,18] Moreover, retro-aldolization is also prone to take place in systems with strong base,[4] whereas medium-strength base is an effective active site for the aldol condensation.[14,19] Notably, acid catalyst sites are found most active for the consecutive dehydration of the aldol product to form C═C bonds.[20]

Zeolite catalysts with unique shape selectivity as well as tuneable acidity and basicity have been introduced for FF aldol condensation.[21] For example, Kikhtyanin et al. applied zeolites with different framework structures (MFI, BEA, FAU and MOR) for the aldol condensation of FF with acetone at 100 °C, however, FF conversions were low (<50 %) in all reactions.[22] Sn-doped MFI and Beta yielded much better performance in the same reaction at 160 °C with the smaller-pore Sn-MFI selectively producing C_8 (61 % yield) and the larger-pore Sn-Beta generating both C_8 (40 % yield) and C_{13} (11 % yield) with high reaction rate.[23] Hence, these studies suggest that metal-doped zeolites may offer both suitable acidity for aldol condensation and appropriate pore size for unique shape selectivity. Amorphous aluminophosphates have also been used in the aldol condensation,[24] but their potential application as metal-doped zeolite/zeotype catalysts remains elusive for such condensation and the relationship between zeotype structure and performance is poorly understood.

In this study, large-pore (8.3 Å) Zr-doped aluminum phosphate (ZrAPOs) with different Zr loadings have been successfully synthesized using a simple hydrothermal method and applied for the cross-aldol condensation of FF (5.6 Å) [25] and CH (5.7 Å) [25] and self-aldol condensation of CH. High C_{11} yield (79.3 %) and C_{16} yield (80.7 %) were obtained for the cross-aldol condensation of FF and CH at 120 °C, whereas 83.3 % C_{12} yield resulted from the self-aldol condensation of CH at 140 °C. A combination of structural and spectroscopic characterization together with elemental analysis demonstrated the successful replacement of P by Zr atoms in the framework sites, providing suitable acidity and basicity to promote the aldol condensations. Adsorption experiments and density functional theory (DFT) calculations unveiled that the introduction of Zr also activated the adsorption of C═O bonds of the substrates. Additionally, the best performing catalyst, i.e. ZrAPO (0.20), was demonstrated to be selective for the conversion of other aldehydes and ketones.

2. Experimental

2.1. Materials

Phosphoric acid 85 % (H_3PO_4, ≥99.8 %), aluminum isopropoxide (Al(O-i-Pr)$_3$, ≥ 98 %), triethylamine (Et_3N, ≥99 %), zirconium acetate solution in dilute acetic acid (15.0–17.0 wt% Zr), furfural (FF, 99 %), 5-methylfurfural (MFA, 99 %), 2,5-furandicarboxaldehyde (FCA, 97 %), benzaldehyde (≥99 %), *m*-tolualdehyde (97%), *p*-tolualdehyde (97 %), *o*-tolualdehyde (97%), acetone (≥99.5 %), 3-pentanone (≥99 %), 4-heptanone (98 %), 5-nonanone (98 %), cyclopentanone (CP, ≥99 %), cyclohexanone (CH, ≥99.0 %), cycloheptanone (CHP, 99%), toluene (≥99.9 %), tetrahydrofuran (THF, ≥99.9 %), 1,4-dioxane (≥99.5 %), and decane (≥99 %) were purchased from Sigma-Aldrich. All chemicals were used as received.

2.2. Catalyst synthesis

The ZrAPO-5 catalysts were prepared as described elsewhere [26,27] using a gel composition of $nZrO_2$:$1Al_2O_3$:$1P_2O_5$:$1Et_3N$:$45H_2O$ (n = 0–0.1). Al(O-i-Pr)$_3$ (14.30 g, 0.07 mol) was added to 23 mL distilled water and the mixture vigorously stirred (1000 rpm) for 0.5 h. Then a solution of 85% H_3PO_4 (8.07 g, 0.07 mol) in 5 mL distilled water was added dropwise and the resulting solution stirred for 1 h. Subsequently, designated amount of zirconium acetate solution (2.00–7.98 g, 3.5–14 mmol) and Et_3N (4.9 mL) were added slowly one by one with intermediate stirring (600 rpm) for 1 h, where after the solution was transferred to an autoclave which was tightly closed and kept at 180 °C under autogenous pressure and static condition for 48 h. After crystallization, the autoclave was cooled to room temperature and the obtained product washed with distilled water several times, oven dried at 110 °C for 12 h and finally calcined at 550 °C for 7 h. ZrAPO-5 with Zr/Al = n was denominated as ZrAPO(n). For example, ZrAPO-5 with Zr/Al = 0.20 (the ratio of the synthesis gel) was denominated as ZrAPO(0.20) (see Table S1 for Zr concentrations in the catalysts). APO-5 was synthesized by an analogous method without addition of the zirconium acetate solution.

2.3. Catalyst characterization

Powder X-ray diffraction patterns (XRD) were recorded at room temperature in transmission mode using Cu-Kα1 radiation from a focusing germanium monochromator and a Huber G760 Guinier in the 2θ interval 3–100 °. The cell parameters of doped samples were refined with the FullProf-WinPLOTR software.[28,29]

Brunauer-Emmett-Teller (BET) surface area and porosity analysis were evaluated by N_2 physisorption performed at − 196 °C by a Micromeritics ASAP 2020 instrument. The samples were degassed at 250 °C for 4 h before the measurement. S_{total} was calculated by the BET method. V_{micro} was estimated by the t-plot method. V_{meso} was calculated by subtraction of the micropore volume from the total pore volume.

X-ray fluorescence (XRF) spectra were measured on a PANalytical εpsilon3-XL instrument. Samples were prepared by fusing them into disks using a Claisse LeNeo fluxer oven.

Ammonia and carbon dioxide temperature-programmed desorption (NH_3-TPD and CO_2-TPD) were performed on a Micromeritics AutoChem II 2920 apparatus. Initially, the samples (0.1 g) were exposed to He gas flow (25 mL/min) and heated up to 600 °C (10 °C/min ramp rate) for 1 h followed by cooling to 100 °C. Then NH_3/CO_2 adsorption were carried out by purging with NH_3/CO_2-He gas mixture (1% NH_3/He; 5 % CO_2/He) for 1 h, where after physically adsorbed gas was removed by purging with He gas for 1 h. Desorption of NH_3/CO_2 was eventually

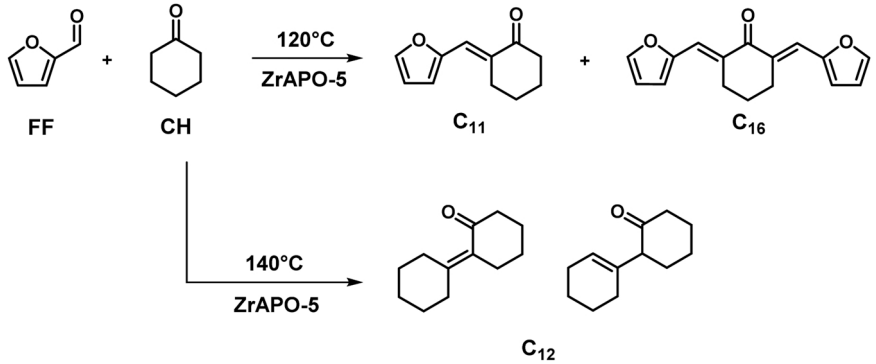

Scheme 1. Strategy for the synthesis of C_{11}, C_{12} and C_{16} fuel precursors with furfural (FF) and cyclohexanone (CH), which can be derived from biomass.

conducted in the temperature range 100/50–600 °C with a heating ramp of 10 °C/min and the amount of liberated gas quantified by a thermal conductivity detector (TCD) and calibration curves.

X-ray photoelectron spectroscopy (XPS) of samples were performed *ex*-situ with a Thermo Scientific system at room temperature using AlKα radiation (1484.6 eV) and a spot size of 400 μm. A flood gun was used to reduce sample charging effects and the obtained spectra were further corrected by setting the C 1s binding energy at 284.8 eV. Data processing was done using the Avantage 4.87 software.

Fourier transformed infrared (FT-IR) spectra of fresh catalysts and catalysts with adsorbed FF or CH were recorded on a Perkin Elmer 100 FT-IR Spectrometer equipped with a Universal ATR sampling accessory. The catalysts with adsorbed FF/CH were prepared by the following method before the measurements: Catalyst (50 mg), FF (96 mg, 1 mmol) or CH (98 mg, 1 mmol) and methanol (1 mL) were mixed and shaken vigorously for 5 min followed by oven drying at 80 °C for 2 h to remove the methanol.

FF and CH temperature-programmed desorption (FF-TPD and CH-TPD) were performed on a Micromeritics AutoChem II 2920 apparatus. The catalysts with FF/CH were prepared by the following method before the measurements: Catalyst (100 mg), FF (192 mg, 2 mmol) or CH (196 mg, 2 mmol) and methanol (1 mL) were mixed and shaken vigorously for 5 min followed by oven drying at 50 °C for 2 h to remove the methanol. Then the samples were transferred for the TPD analysis. Desorption of FF/CH was eventually conducted in the temperature range 50–600 °C with a heating ramp of 10 °C/min.

^{27}Al and ^{31}P magic-angle spinning nuclear magnetic resonance (MAS NMR) spectra were recorded on a Bruker AVANCE III HD spectrometer and operated at a magnetic field of 14.05 T equipped with a 4 mm CP/MAS BBFO probe.

Scanning electron microscopy (SEM) images of samples were recorded on an AFEG 250 Analytical ESEM at 5 kV.

2.4. Catalyst activity tests

Cross- and self-aldol condensation reactions were conducted in 15 mL ACE pressure tubes in an oil bath with a magnetic stirrer. A mixture of FF, catalyst and CH, or a mixture of CH and catalyst, was added to the tube and the tube placed in an oil bath (600 rpm) with a designated reaction temperature. After a specified reaction time, the tube was cooled to room temperature and a liquid sample of the reaction mixture diluted with acetone to 10 mL in a volumetric flask followed by analysis (decane as an internal standard) using gas chromatography-mass spectrometry (GC-MS) (Agilent 6850–5975 C) with GC flame-ionization detection (GC-FID) (Agilent 6890 N), both equipped with an HP-5MS capillary column (30.0 m × 250 μm × 0.25 μm). A mixture of H_2 with a flow rate of 30 mL/min and N_2 with a flow rate of 25 mL/min was used as a carrier gas. The sample injection volume was 1 μL. The injection port temperature was 270 °C. The oven was temperature programmed to start at 40 °C for 1 min, ramp with 10 °C/min to 200 °C, ramp with 5 °C/min to 270 °C, and then hold at this temperature for 5 min. The temperature of the FID was 270 °C.

The calibration of all substrates and products was quantified based on the response factor method proposed by Scanlon and Willis.[30] The cross-aldol condensation products consisted of two possible geometrical isomers of C_{11} (*cis* and *trans*) and three of C_{16} (double *cis*, *cis-trans*, and double *trans*) (Fig. S1). Likewise, the self-aldol condensation products consisted of two possible structural isomers of C_{12} and three isomers of C_{18} (Fig. S2). All isomers were quantified together when calculating the selectivity and yield.

2.5. Catalyst recycling test

The reusability of ZrAPO(0.20) was examined for the cross-aldol condensation of FF and CH in the neat reaction system at 120 °C after 1 h reaction. After initial reaction, the catalyst was collected via centrifugation (12,000 rpm, 5 min), washed with methanol and acetone twice (2 × 10 mL), respectively, followed by drying at 80 °C for 2 h before being reused. After three reaction runs, the catalyst was collected via centrifugation (12,000 rpm, 5 min), dried and calcined at 550 °C for 4 h before being used in the next reaction run. The reusability of ZrAPO (0.20) in the analogous reaction system with toluene was examined at 120 °C after 4 h reaction. After reaction, the catalyst was collected and washed by using the aforementioned method, and after the first two reaction runs the catalyst was also calcined.

2.6. Theoretical calculations

2.6.1. Models

The bulk structure of APO-5 was adapted from the Material Project.[31] Considering the relative size of the catalyst pores and the FF and CH molecules, the primitive unit structure of 1 × 1 × 1 APO-5 was applied as the model. Note that in the unit cell of APO-5, all Al or P atoms have identical chemical environments.

To simulate the ZrAPO catalysts in the experiments, one Zr atom was replaced with one P atom to form the Zr-doped APO-5 model and the structure was fully relaxed before adding adsorbates, ca. 0.08 Zr/Al molar ratio was used per unit cell in the model. The model of APO-5 was restructured a bit after Zr substitution due to the different chemical coordination of P and Zr atoms.

2.6.2. DFT parameters

Density functional theory (DFT) calculations were carried out using Vienna Ab initio Software Package (VASP).[32] The calculations employed the generalized gradient approximation (GGA) [33] in the form of the Bayesian error estimation functional with van der Waals correlation (BEEF-vdW) [34], which was reported to exhibit good description for the interaction between adsorbates and surfaces.[35,36] Moreover, Goncalves et al. recently benchmarked the accuracy of DFT functionals in zeolite catalysis and showed that BEEF-vdW displays good accuracy in quantifying adsorption strength of organic species in zeolites at GGA level.[37]

The projector augmented wave (PAW) method [38] was applied to describe the interaction between the atomic cores and valence electrons. The geometries of both zeolites and adsorbates in the calculations were relaxed until the force on every atom was less than 0.02 eV/Å with a cutoff energy of 500 eV. Considering the bulk structure of the zeolite, a k-points set of 3 × 3 × 3 was applied in all calculations after the convergence test. The adsorption energy ΔE of CH or FF was calculated as below:

$$\Delta E = E_{total} - E_{zeolite} - E_{CH/FF}$$

Where E_{total} is the calculated total energy of adsorption system, $E_{zeolite}$ is the calculated energy of the zeolite structure without adsorbates and $E_{CH/FF}$ is the calculated energy of the CH or FF molecules.

3. Results and discussion

3.1. Structure of catalysts

XRD patterns of the synthesized APO-5 and ZrAPOs (Fig. 1a) confirmed that all materials possessed a well-crystalline AFI structure without impurities such as, ZrO_2.[39–41] For the ZrAPOs were all distinctive peaks slightly shifted (several high intensity peaks shown in zoom), and when the peaks were used to calculate the unit cell volumes a positive relationship with Zr/Al ratios were found (Table S2 and Fig. 1b). The larger atom radius of Zr (0.59 Å) compared to that of Al (0.39 Å) and P (0.17 Å) expanded the unit cell volumes,[42] as also seen by comparing the calculated optimized structures of APO-5 with or without Zr doping (Figs. S3 and S4). Furthermore, nitrogen physisorption confirmed both APO-5 and ZrAPOs to be microporous with

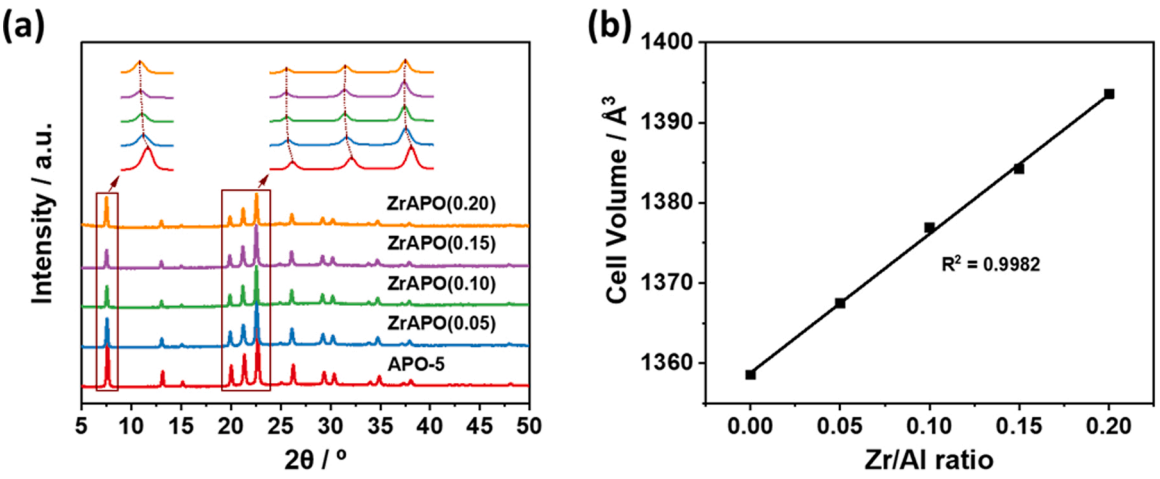

Fig. 1. (a) XRD patterns of APO-5 and ZrAPO catalysts, and (b) the relationship between Zr/Al ratio and cell volume in the catalysts.

type I isotherms (Fig. S5), and the microporous volume was reduced while the mesoporous volume was enhanced with increased Zr loading. This also resulted in variations of surface area (Table 1), and indicated that some intercrystalline pores may have formed at high Zr loading ($n > 0.15$).

SEM results showed that the morphology of the materials changed from hexagon prism-like shape with 3–4 μm particle size (APO-5) to around 18 μm spherical agglomerates made of rodlike shaped particles for ZrAPO(0.05) (Fig. 2a-c), which was likely caused by differences in pH of the gel [43] during synthesis induced by the varied zirconium acetate concentrations. EDX mapping further suggested a homogeneous distribution of elements in the ZrAPO samples (Fig. 2d-h).

Characterization by XPS, FT-IR, solid-state MAS NMR and XRF were used to understand the state of Zr in the ZrAPOs. The reference ZrO_2 revealed by XPS (Fig. 3a) two distinct peaks at 181.0 and 183.4 eV assigned to Zr $3d_{5/2}$ and Zr $3d_{3/2}$, respectively. For the ZrAPOs, these peaks were shifted to higher binding energy (182.5 and 184.9 eV) implying the incorporation of tetrahedrally coordinated Zr atoms into the framework.[44,45] Additionally, in FT-IR spectra of the catalysts a shift of the Al-O-P band from 1108 cm^{-1} (APO-5) to 1074 cm^{-1} (ZrAPO (0.20)) (Fig. 3b) indicated the replacement of Al or P for Zr,[46] Furthermore, a new peak at around 3668 cm^{-1} assigned to terminal P-OH groups [47–49] appeared after the incorporation of Zr, which was also in line with results obtained by ^{27}Al and ^{31}P solid-state MAS NMR spectroscopy (Fig. S6), where a broad peak belonging to P-OH defect groups [47,50] was formed after the introduction of Zr with a positive area relationship to the metal content. Moreover, the Al/P molar ratio increased with increasing Zr loading (Table 1) indicating loss of P atoms during the substitution probably due to the replacement of P by Zr atoms in framework sites. This result is consistent with previous findings that P can be substituted by elements with valence from + 1 to + 5, while aluminium atoms can be replaced with atoms of valence + 1 to + 3.[51] To sum up, Zr atoms were successfully substituted in the framework of the ZrAPO catalysts presumable by replacing P atoms resulting in the formation of terminal P-OH groups (Scheme S1).

3.2. Cross-aldol condensation of furfural and cyclohexanone

Both APO-5 and ZrAPOs were catalytically active in the cross-aldol condensation of FF with CH (Fig. 4a) towards two main products; a first adduct (C_{11}) and a second adduct (C_{16}) obtained from the consecutive reaction of C_{11} and FF (Scheme 1). No intermediate C_{11} or C_{16} alcohols were observed, indicating fast dehydration of these alcohols to α,β-unsaturated ketone products. Compared to APO-5 the ZrAPOs exhibited better catalytic performance resulting in both higher FF conversions and C_{11}/C_{16} selectivities, and ZrAPO(0.20) displayed the highest catalytic activity which was probably related to its suitable acidity and basicity (vide infra).[52–54] Moreover, increased CH concentrations promoted the aldol condensation between FF and CH, while the aldol condensation of FF and C_{11} was suppressed leading to high C_{11} selectivity and low C_{16} selectivity (Fig. 4b). Thus, an optimal CH:FF ratio of 1:10 in ZrAPO(0.20) catalyst resulted in 79.3 % C_{11} yield and 16.4 % C_{16} yield with 99.2 % FF conversion after 3 h of reaction. Notably, with FF:CH ratios lower than 1:2 a yellow solid product formed during reaction, which might be precipitated C_{11} and C_{16} as also reported in similar studies.[7,55] The formation of this solid product reduced the interaction between the catalyst and the substrates thus like disrupting the reaction.

The effect of solvents was further explored in the cross-aldol condensation reaction with the ZrAPO(0.20) catalyst. As shown in Fig. 4c, all the reactions with solvents led to lower FF conversion possibly due to the lower substrate concentrations obtained after dilution. Especially, water resulted in significant lower product selectivity as well as large carbon loss compared to the neat reaction system, which

Table 1
Physicochemical properties of the APO-5 and ZrAPOs catalysts.

Sample	Zr/Al ratio[a]	Zr/P ratio[a]	Al/P ratio[a]	S_{total} (m^2/g)[b]	V_{micro} (cm^3/g)[b]	V_{meso} (cm^3/g)[b]	Acidity (mmol/g)[c]	Basicity (mmol/g)[d]
APO-5	–	–	0.95	197	0.07	0.11	0.0012	0.04
ZrAPO(0.05)	0.04	0.04	0.93	184	0.06	0.13	0.24	0.17
ZrAPO(0.10)	0.07	0.08	1.10	223	0.07	0.15	0.31	0.21
ZrAPO(0.15)	0.13	0.16	1.17	224	0.05	0.21	0.42	0.28
ZrAPO(0.20)	0.16	0.21	1.36	203	0.03	0.29	0.52	0.34

[a] Determined by XRF.
[b] Determined by N_2 physisorption.
[c] Determined by NH_3-TPD.
[d] Determined by CO_2-TPD.

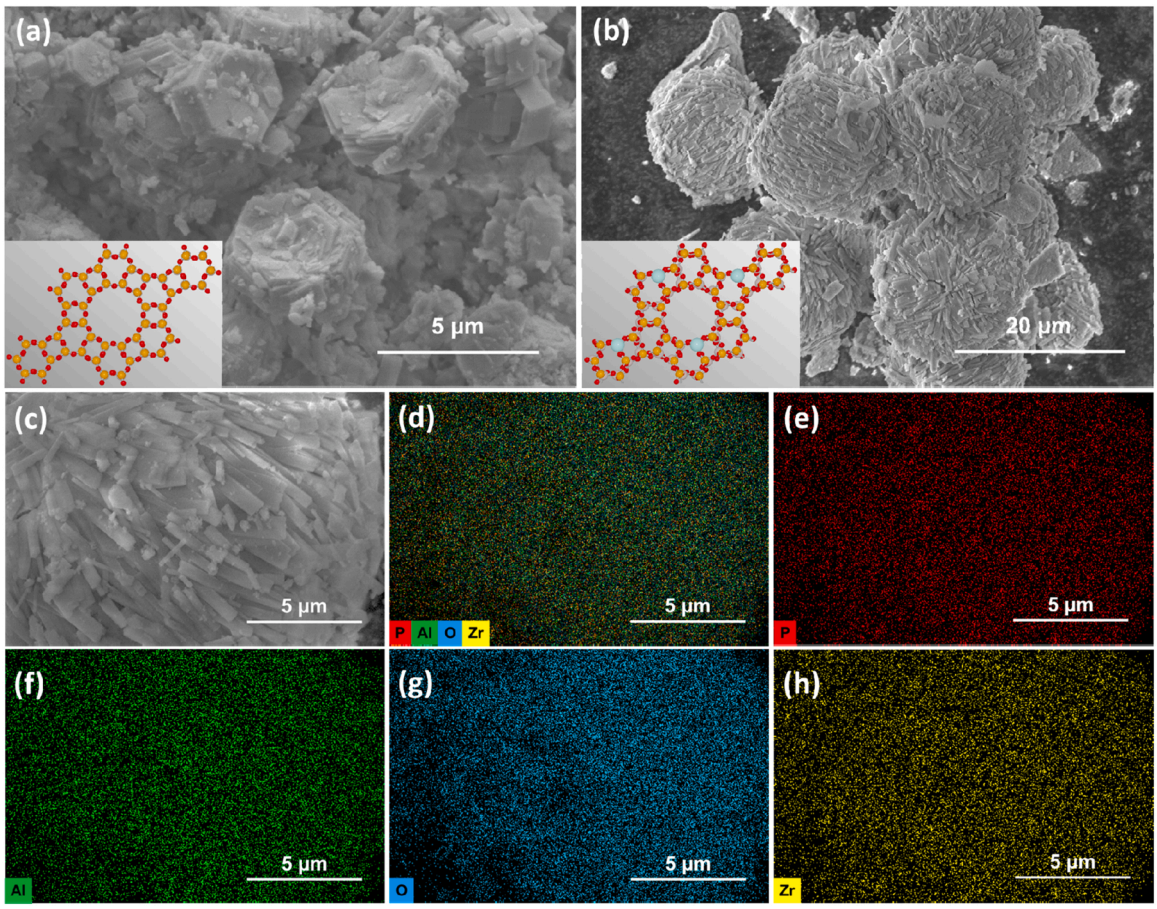

Fig. 2. SEM images of (a) APO-5, (b) and (c) ZrAPO(0.05) (inset: Computational models; P atom: yellow; Al atom: gray; O atom: red; Zr atom: light blue). (d)-(h) EDX mapping analysis on ZrAPO(0.05).

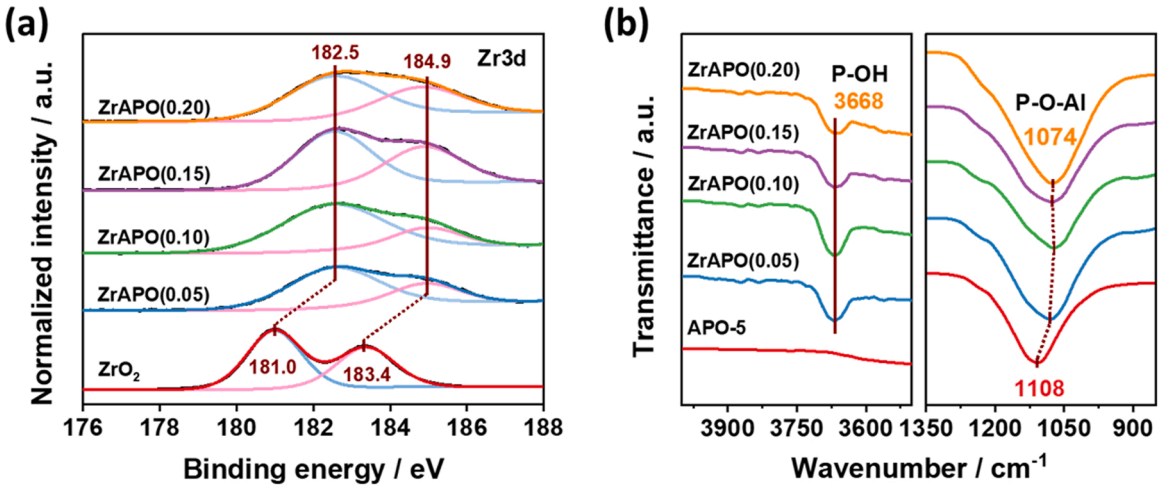

Fig. 3. (a) Zr 3d XPS spectra of ZrO_2 and ZrAPO catalysts. (b) FT-IR spectra of APO-5 and ZrAPO catalysts.

might be due to poor FF/product solubility [55] or side reactions such as polymerization and decomposition.[56] Noticeably, the use of 1, 4-dioxane and toluene solvent increased the C_{16} selectivity and the lower CH concentration facilitated the consecutive condensation between FF and C_{11} giving rise to 80.7 % C_{16} yield in toluene.

3.3. Catalyst recycling

In recycling experiments, the ZrAPO(0.20) catalyst exhibited deactivation in the neat reaction system after the first three reaction runs with only intermediate acetone/methanol washing, resulting in a decline in yield of C_{11} from 61.2% to 37.4% (Fig. 5a). However, the original catalytic performance restored completely in successive catalytic runs after calcination. Oppositely, severe catalyst deactivation

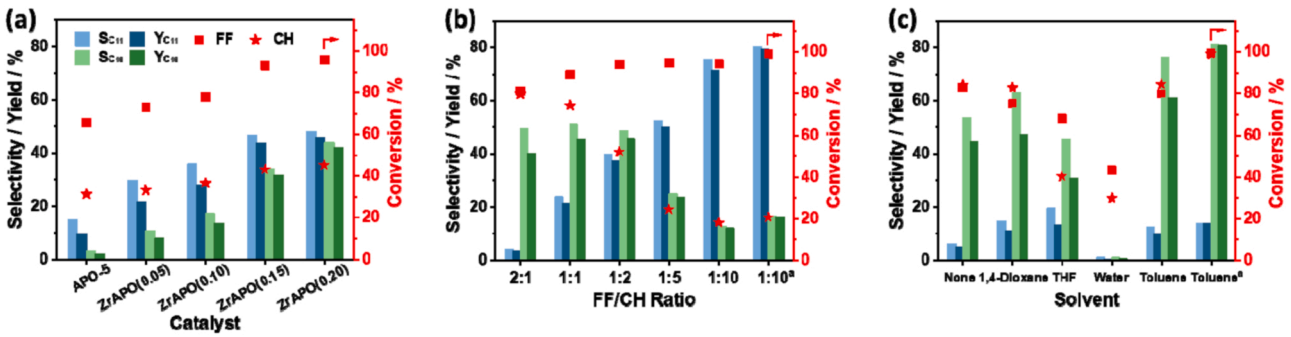

Fig. 4. Catalytic results from cross-aldol condensation of FF and CH using (a) different catalysts (reaction conditions: FF (166 μL, 2 mmol), catalyst (50 mg), CH (515 μL, 5 mmol), 120 °C, 2 h), (b) different FF to CH ratios with ZrAPO(0.20) catalyst (reaction conditions: FF (166 μL, 2 mmol), ZrAPO(0.20) (50 mg), CH (1–20 mmol), 120 °C, 2 h or [a]3 h) and (c) different solvents with ZrAPO(0.20) catalyst (reaction conditions: FF (166 μL, 2 mmol), ZrAPO(0.20) (50 mg), CH (103 μL, 1 mmol), solvent (1 mL) 120 °C, 4 h or [a]12 h).

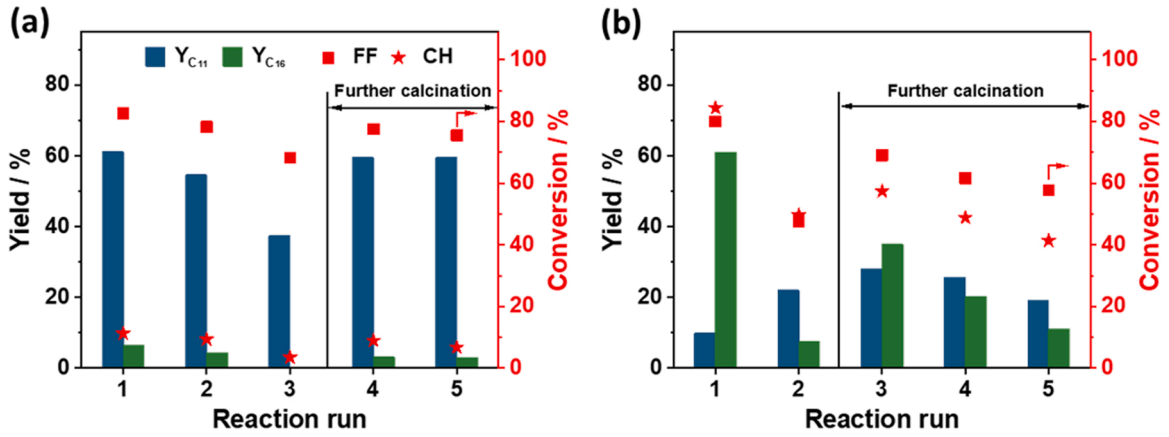

Fig. 5. Recyclability of ZrAPO(0.20) catalyst in the cross-aldol condensation reaction of FF with CH (reaction conditions: (a) FF (166 μL, 2 mmol), ZrAPO(0.20) (50 mg), CH (2060 μL, 20 mmol), 120 °C, 1 h; (b) FF (166 μL, 2 mmol), ZrAPO(0.20) (50 mg), CH (103 μL, 1 mmol), toluene (1 mL), 120 °C, 4 h).

prevailed in the toluene system after washing as well as further calcination resulting in significantly decreased C_{16} yield, while more C_{11} product apparently formed (Fig. 5b). TG analysis of the used ZrAPO (0.20) catalyst in the two reaction systems showed a mass loss (6.8 and 15.2 wt%, respectively) with broad peaks around 326 °C and 497 °C (Fig. S7). Moreover, the FT-IR spectrum of the used catalyst revealed

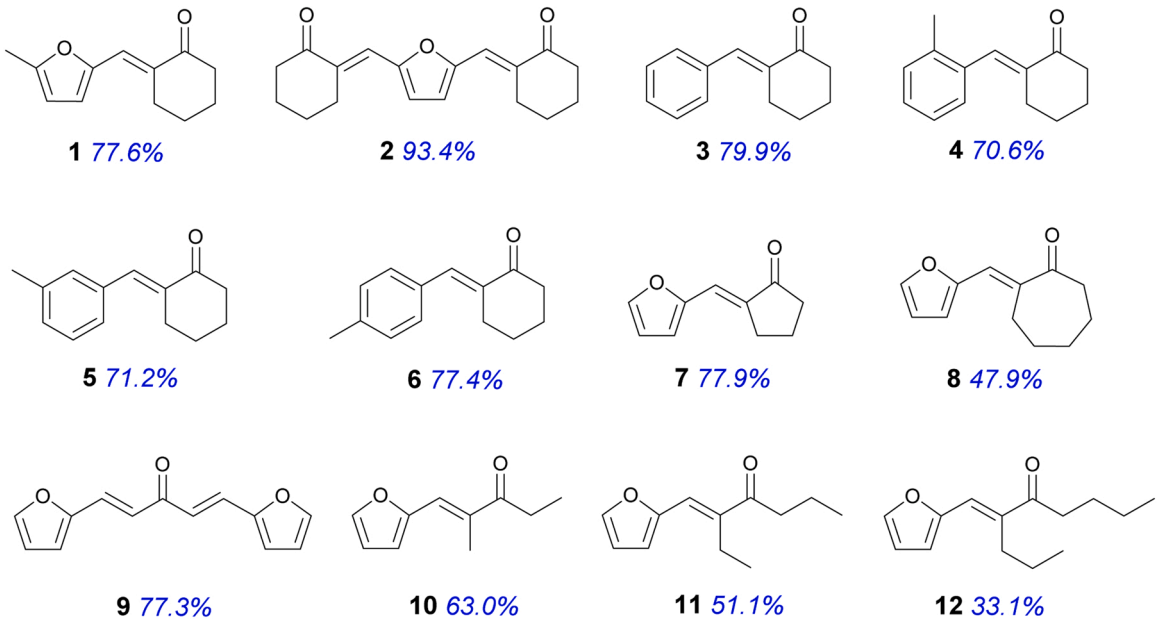

Fig. 6. Products formed by cross-aldol condensation of various carbonyl compounds using ZrAPO(0.20) catalyst (see Table S4 for reaction conditions).

bands around 1621 cm^{-1} (C═C stretching vibration) as well as 2940 and 1461 cm^{-1} (C-H vibrations) (Fig. S8) along with reduced surface area and pore volume (Table S3). In both systems, the catalyst framework structure also remained the same after several calcinations as shown by XRD analysis (Fig. S9). Combined these results suggest that adsorption of organic species on active catalyst sites partly induced deactivation and pore blocking in both systems, which could be removed by calcination (550 °C). For the toluene system, additional formation of polymerization products of FF might account for more severe deactivation.

3.4. Substrate scope

The ZrAPO(0.20) catalyst also showed very promising catalytic performance for cross-aldol condensation of other carbonyl compounds besides FF and CH (Fig. 6; see Table S4 for reaction conditions). For example, 77.6 % yield of **1** was obtained by the condensation of 5-methylfurfural and CH, which was similar to the C_{11} yield obtained with FF and CH, and 93.4% yield of **2** obtained from reaction of 2,5-furandicarboxaldehyde with CH at high CH concentration. Also aromatic aldehydes such as *m*-tolualdehyde, *p*-tolualdehyde, and *o*-tolualdehyde gave good yields (>70 %) with CH of the corresponding products **3**, **4**, **5**, and **6** after extended reaction time (24 h). The yield of **7** obtained with the alternative cyclic ketone cyclopentanone and FF was also similar to the C_{11} yield with FF and CH, while the corresponding yield of **8** with cycloheptanone was lower probably due to the larger ring size of cycloheptanone limited the reaction.[14] Open-chain aliphatic ketones provided lower yields than cyclic ketones despite prolonged reaction time as also reported in other studies,[57] and with FF and acetone was **9** preferentially formed with the pore size of ZrAPO(0.20) in agreement with a previous study using Sn-Beta catalyst.[23] The lower product yields of **10**, **11** and **12** (33–63 %) obtained with 3-pentanone, 4-heptanone and 5-nonanone, respectively, was probably a result of the larger steric effects caused by the methyl, ethyl and propyl group in the α-carbon position [4] as well as lower reactivity of the α-carbon atom in the longer carbon chain.[58]

3.5. Self-aldol condensation of cyclohexanone

The APO-5 and ZrAPOs catalysts were also applied for the self-condensation of CH at 140 °C with larger amount of catalyst than used for the cross-condensation of FF and CH (Fig. 7). Two products formed in the systems; a first adduct (C_{12}, Scheme 1) and a minor amount of a second adduct (C_{18}) obtained from the consecutive reaction of C_{12} and CH. As for the cross-aldol condensation of FF and CH, all the ZrAPOs catalysts exhibited better catalytic performance than APO-5 and also here ZrAPO(0.20) provided the best catalyst performance, which after reaction optimization (increased catalyst amount and longer reaction time) resulted in a C_{12} yield of 83.3 % with a 92.2 % CH conversion.

3.6. The role of Zr in the aldol condensations

FT-IR spectra of the APO-5 and ZrAPOs catalysts with pre-adsorbed FF or CH were recorded to get insight into the origin of the different catalytic performances. Surface adsorbed FF had a strong intensity of the *ν*(C═O) stretching band, while the furan ring breath and *ν*(C═C) stretching bands were much less intense (Fig. 8a), suggesting that the carbonyl group was the main adsorptive functional group of FF.[59,60] Moreover, an obvious red-shift of the *ν*(C═O) band from 1668 to 1663 cm^{-1} on APO-5 and to 1661 cm^{-1} on ZrAPO(0.20) was observed for the surface adsorbed FF, implying that the C═O group of FF was activated by the adsorption.[59,61] For the CH adsorption a red-shift of *ν* (C═O) also suggested that CH interacted with the catalysts with the C═O functional group (Fig. 8b),[62] thus confirming that adsorption of the C═O group of both FF and CH on the catalysts promoted the aldol condensation.

TPD experiments and DFT calculations were additionally carried out to evaluate the difference in adsorption strength of FF and CH on the APO-5 and ZrAPOs catalysts. FF-TPD and CH-TPD profiles (Fig. 9a-b) showed that the ZrAPOs had higher desorption temperature of both FF and CH than APO-5, suggesting that the presence of Zr faciliated the adsorption of FF and CH on the catalysts.[63] Meanwhile, the optimized FF and CH adsorption configurations and adsorption energies calculated for APO-5 and ZrAPO with FF and CH in the large 12-membered rings are depicted in Fig. 9c. For APO-5, both CH and FF had only relatively weak adsorptive interaction with the surface. In contrast, the molecules interacted stronger with the surface of ZrAPO with activated adsorption via the terminal O atom in C═O group resulting in larger adsorption strengths. Notably, FF displayed a twice as large adsorption energy enhancement (0.23 eV) compared to CH (0.11 eV) after Zr doping, implying that the Zr incorporation preferentially promoted adsorption of FF and thus cross-aldol condensation reaction of FF and CH rather than self-aldol condensation of CH, as also observed experimentally in Fig. 4a.

3.7. The role of acidity/basicity in the aldol condensations

Previous studies have shown that aldol condensations can be base- or acid-base co-catalyzed.[52–54] Herein, the FF consumption rate and C_{11} and C_{16} formation rates had positive relationships with both acidity and

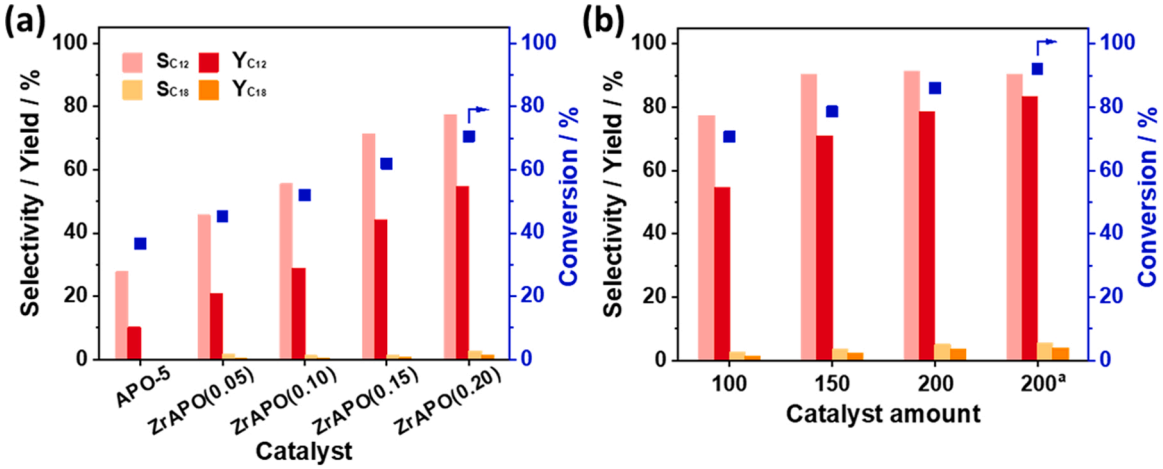

Fig. 7. Catalytic results from CH self-condensation with (a) different catalysts (reaction conditions: CH (515 μL, 5 mmol), catalyst (100 mg), 140 °C, 48 h) and (b) different amounts of ZrAPO(0.20) catalyst (reaction conditions: CH (103 μL, 5 mmol), 140 °C, 48 h or [a]72 h).

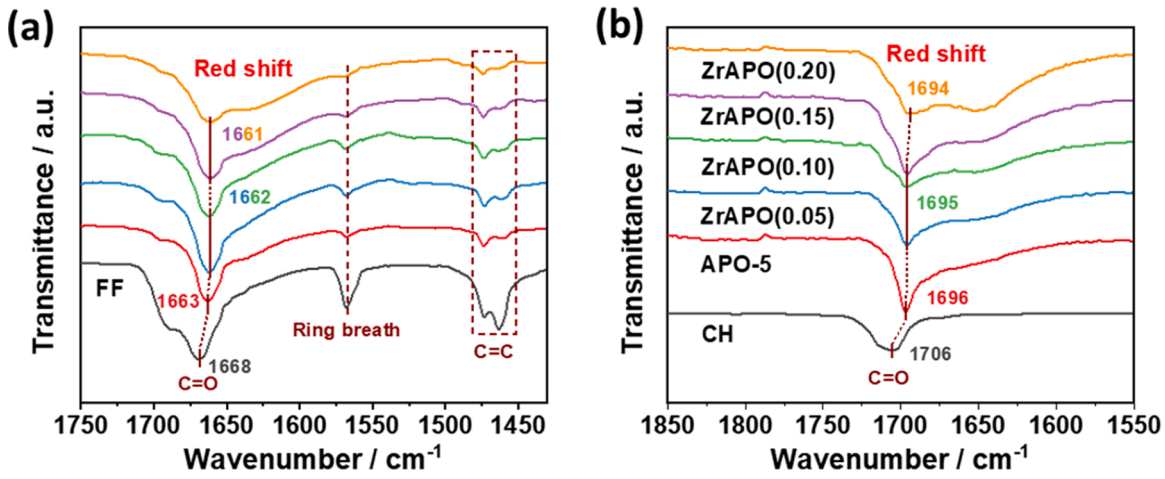

Fig. 8. FT-IR spectra of APO-5 and ZrAPOs catalysts with pre-adsorbed (a) FF and (b) CH.

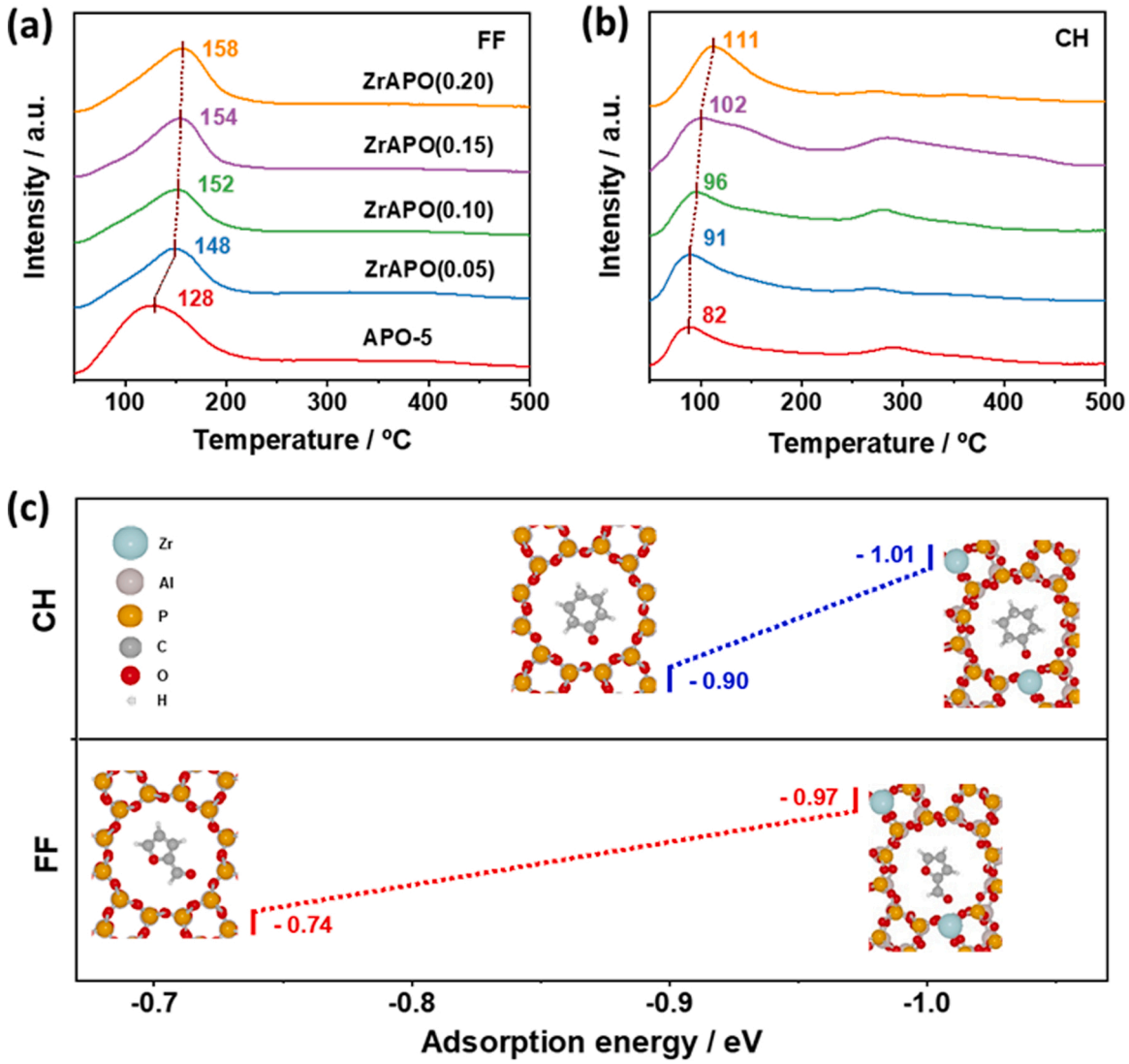

Fig. 9. TPD profiles of APO-5 and ZrAPO catalysts with (a) FF and (b) CH. (c) The calculated adsorption energies (eV) of FF and CH on APO-5 (left) and ZrAPO (right) models. Color codes of the different atoms are inserted in the upper panel.

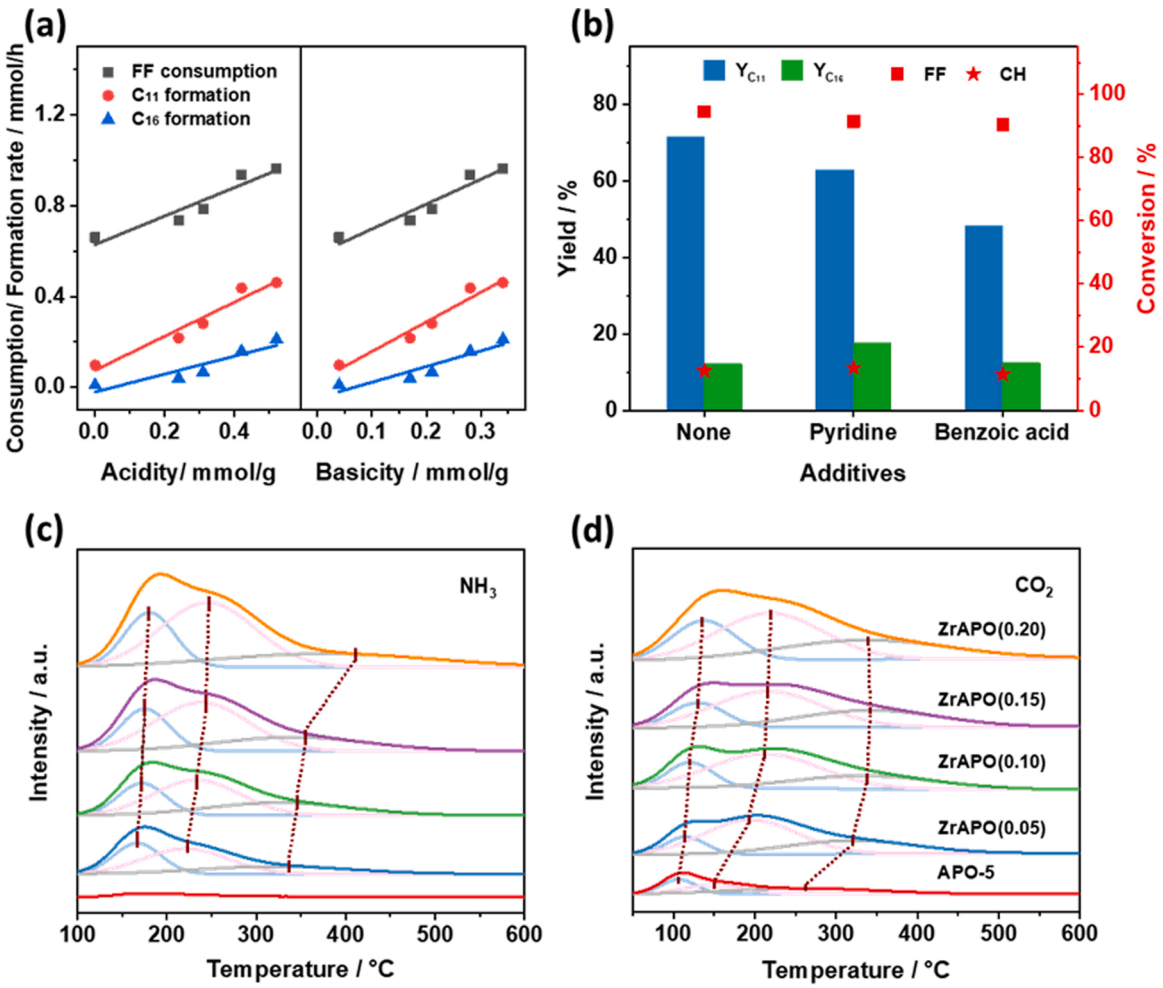

Fig. 10. (a) The correlation between acidity/basicity and FF consumption rate/product formation rate. (b) Poisoning reaction of cross-aldol condensation of FF and CH with ZrAPO(0.20) catalyst (reaction conditions: FF (192 mg, 2 mmol), ZrAPO(0.20) (50 mg), additive (100 mg), CH (2060 μL, 20 mmol), 120 °C, 2 h). (c) NH_3-TPD and (d) CO_2-TPD profiles of APO-5 and ZrAPO catalysts.

basicity of catalysts (Fig. 10a). Poisoning reactions with pyridine and benzoic acid led to decreased yield of both C_{11} and C_{16} products, implying that the cross-aldol condensation of FF and CH was catalyzed both by acid and base with ZrAPO(0.20) catalyst (Fig. 10b).

NH_3-TPD (Fig. 10c) revealed that APO-5 possessed only a low amount of weak acid sites (small peak at 164 °C; Table S5) consistent with the assumption that APO-5 is neutral. In contrast, the ZrAPO catalysts displayed much higher acid density and acid strength (larger peaks at 220–250 °C and 320–380 °C; Table S5), possibly due to terminal P-OH and bridged hydroxyl groups, i.e., Zr-OH-Al.[48,49] Likewise, CO_2-TPD results (Fig. 10d, Table S6) confirmed that the basicity and strength of the basic catalyst sites also increased, which might origin from the negatively charged lattice oxygen atoms (Zr-O$^-$-Al) after Zr incorporation.[64,65] Hence, the superior aldol condensation

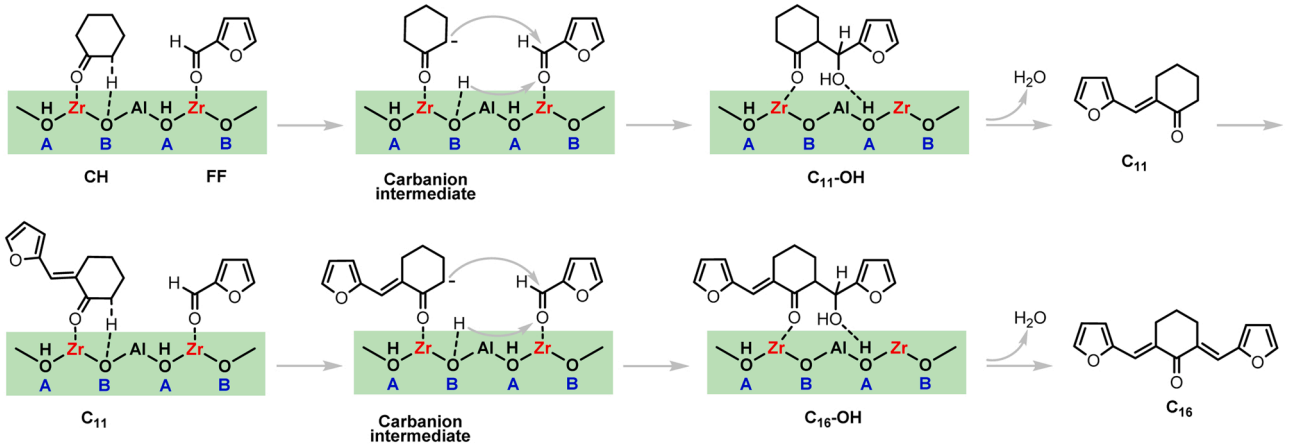

Scheme 2. Possible reaction pathways for the cross-aldol condensation of FF with CH with ZrAPO(0.20) catalyst.

performance facilitated by the Zr incorporation was possibly due to the enhanced adsorption strength of substrates, and a combination of basic sites promoting α-proton abstraction of CH to form a carbanion intermediate followed by reaction with the carbonyl group of the adsorbed FF, [13] and the presence of acid sites promoting the subsequent dehydration to form the products (Scheme 2).[4]

4. Conclusions

In this work, Zr-doped aluminum phosphates (ZrAPOs) with Zr substitution of P in the zeolite framework have been shown to promote the aldol condensation of FF and CH. The best catalyst ZrAPO(0.20) yielded up to 79.3 % C_{11} and 80.7 % C_{16} in the cross-aldol condensation of FF and CH and sustained high activity for five consecutive reactions run with intermediate calcination, which is superior performance to previously reported catalyst systems (Table S7). Furthermore, ZrAPO (0.20) proved generally applicable for the cross-aldol condensation of other ketones and aldehydes as well as for the self-aldol condensation of CH, where 83.3 % C_{12} yield with 92.2 % CH conversion was realized.

Structure-performance relationship between Zr-doping and the promoted reactivity was further established: 1) Both adsorption experiments and DFT calculations demonstrated that the introduction of Zr enhanced the adsorption strength of FF and CH via the carbonyl group interacting with Zr, further facilitating the aldol condensation reactions, and 2) the correlation between reaction rate and acidity/basicity and poisoning reaction proved that increased acidity and basicity by Zr substitution in the framework of APO-5 co-catalyzed the aldol condensation, facilitating the good yield of C_{11}, C_{12} and C_{16}.

In perspective, this work introduces efficient routes for the synthesis of diesel and jet fuel range intermediates C_{11}, C_{12} and C_{16} from FF and CH via metal-doped zeotype catalysis, which presents efficient avenues to convert biomass-derived feedstocks.

CRediT authorship contribution statement

Wenting Fang: Conceptualization, Methodology, Investigation, Visualization, Writing – original draft. **Sihang Liub:** Methodology, Investigation, Writing – original draft. **Leonhard Schill:** Resources, Investigation. **Mariusz Kubus:** Resources, Data curation. **Thomas Bligaard:** Resources, Writing – review & editing. **Anders Riisager:** Conceptualization, Writing – review & editing, Supervision, Project administration.

Declaration of Competing Interest

The authors declare that they have no known competing financial interests or personal relationships that could have appeared to influence the work reported in this paper.

Data Availability

Data will be made available on request.

Acknowledgements

W.F. acknowledges the China Scholarship Council, China (No. 201908330324) for awarding a scholarship and the Department of Chemistry, Technical University of Denmark, Denmark is acknowledged for supporting the work. S.L. acknowledges the research grant (29450) from Villum Fonden, Denmark and the Department of Physics, Technical University of Denmark, Denmark.

Appendix A. Supporting information

Supplementary data associated with this article can be found in the online version at doi:10.1016/j.apcatb.2022.121936.

References

[1] D.M. Alonso, J.Q. Bond, J.A. Dumesic, Catalytic conversion of biomass to biofuels, Green Chem. 12 (2010) 1493–1513.
[2] J.Q. Bond, A.A. Upadhye, H. Olcay, G.A. Tompsett, J. Jae, R. Xing, D.M. Alonso, D. Wang, T.Y. Zhang, R. Kumar, A. Foster, S.M. Sen, C.T. Maravelias, R. Malina, S. R.H. Barrett, R. Lobo, C.E. Wyman, J.A. Dumesic, G.W. Huber, Production of renewable jet fuel range alkanes and commodity chemicals from integrated catalytic processing of biomass, Energy Environ. Sci. 7 (2014) 1500–1523.
[3] Y. Jing, Y. Guo, Q. Xia, X. Liu, Y. Wang, Catalytic production of value-added chemicals and liquid fuels from lignocellulosic biomass, Chem 5 (2019) 2520–2546.
[4] H. Li, A. Riisager, S. Saravanamurugan, A. Pandey, R.S. Sangwan, S. Yang, R. Luque, Carbon-increasing catalytic strategies for upgrading biomass into energy-intensive fuels and chemicals, ACS Catal. 8 (2017) 148–187.
[5] Q. Meng, M. Hou, H. Liu, J. Song, B. Han, Synthesis of ketones from biomass-derived feedstock, Nat. Commun. 8 (2017) 14190.
[6] X. Li, P. Jia, T. Wang, Furfural: A promising platform compound for sustainable production of C4 and C5 chemicals, ACS Catal. 6 (2016) 7621–7640.
[7] O. Kikhtyanin, D. Kadlec, R. Velvarska, D. Kubicka, Using Mg-Al mixed oxide and reconstructed hydrotalcite as basic catalysts for aldol condensation of furfural and cyclohexanone, ChemCatChem 10 (2018) 1464–1475.
[8] J. Yang, N. Li, G. Li, W. Wang, A. Wang, X. Wang, Y. Cong, T. Zhang, Synthesis of renewable high-density fuels using cyclopentanone derived from lignocellulose, Chem. Commun. 50 (2014) 2572–2574.
[9] R.E. O'Neill, L. Vanoye, C. De Bellefon, F. Aiouache, Aldol-condensation of furfural by activated dolomite catalyst, Appl. Catal. B: Environ. 144 (2014) 46–56.
[10] N. Fakhfakh, P. Cognet, M. Cabassud, Y. Lucchese, M.D. de Los Ríos, Stoichio-kinetic modeling and optimization of chemical synthesis: application to the aldolic condensation of furfural on acetone, Chem. Eng. Process. 47 (2008) 349–362.
[11] R.M. West, Z.Y. Liu, M. Peter, C.A. Gartner, J.A. Dumesic, Carbon-carbon bond formation for biomass-derived furfurals and ketones by aldol condensation in a biphasic system, J. Mol. Catal. A-Chem. 296 (2008) 18–27.
[12] M. Hronec, K. Fulajtárova, T. Liptaj, M. Štolcová, N. Prónayová, T. Soták, Cyclopentanone: a raw material for production of C_{15} and C_{17} fuel precursors, Biomass Bioenergy 63 (2014) 291–299.
[13] L. Faba, E. Diaz, S. Ordonez, Aqueous-phase furfural-acetone aldol condensation over basic mixed oxides, Appl. Catal. B: Environ. 113 (2012) 201–211.
[14] J. Cueto, L. Faba, E. Díaz, S. Ordóñez, Performance of basic mixed oxides for aqueous-phase 5-hydroxymethylfurfural-acetone aldol condensation, Appl. Catal. B: Environ. 201 (2017) 221–231.
[15] A. Tampierr, C. Russo, R. Marotta, M. Constanti, S. Contreras, F. Medina, Microwave-assisted condensation of bio-based hydroxymethylfurfural and acetone over recyclable hydrotalcite-related materials, Appl. Catal. B: Environ. 282 (2021), 119599.
[16] D. Liang, G. Li, Y. Liu, J. Wu, X. Zhang, Controllable self-aldol condensation of cyclopentanone over MgO-ZrO_2 mixed oxides: Origin of activity & selectivity, Catal. Commun. 81 (2016) 33–36.
[17] O. Kikhtyanin, E. Lesnik, D. Kubička, The occurrence of Cannizzaro reaction over Mg-Al hydrotalcites, Appl. Catal. A: Gen. 525 (2016) 215–225.
[18] J.L. Xu, N. Li, X.F. Yang, G.Y. Li, A.Q. Wang, Y. Cong, X.D. Wang, T. Zhang, Synthesis of diesel and jet fuel range alkanes with furfural and angelica lactone, ACS Catal. 7 (2017) 5880–5886.
[19] X. Kong, X.J. Wei, L.P. Li, Z. Fang, H.W. Lei, Production of liquid fuel intermediates from furfural via aldol condensation over $La_2O_2CO_3$-ZnO-Al_2O_3 catalyst, Catal. Commun. 149 (2021), 106207.
[20] D. Nguyen Thanh, O. Kikhtyanin, R. Ramos, M. Kothari, P. Ulbrich, T. Munshi, D. Kubička, Nanosized TiO_2—a promising catalyst for the aldol condensation of furfural with acetone in biomass upgrading, Catal. Today 277 (2016) 97–107.
[21] J.D. Lewis, S. Van de Vyver, Y. Roman-Leshkov, Acid-base pairs in Lewis acidic zeolites promote direct adol reactions by soft enolization, Angew. Chem. 127 (2015) 9973–9976.
[22] O. Kikhtyanin, V. Kelbichova, D. Vitvarova, M. Kubu, D. Kubicka, Aldol condensation of furfural and acetone on zeolites, Catal. Today 227 (2014) 154–162.
[23] M.X. Su, W.Z. Li, T.W. Zhang, H.S. Xin, S. Li, W. Fan, L.L. Mac, Production of liquid fuel intermediates from furfural via aldol condensation over Lewis acid zeolite catalysts, Catal. Sci. Technol. 7 (2017) 3555–3561.
[24] A. Hamza, N. Nagaraju, Amorphous metal-aluminophosphate catalysts for aldol condensation of n-heptanal and benzaldehyde to jasminaldehyde, Chin. J. Catal. 36 (2015) 209–215.
[25] J. Jae, G.A. Tompsett, A.J. Foster, K.D. Hammond, S.M. Auerbach, R.F. Lobo, G. W. Huber, Investigation into the shape selectivity of zeolite catalysts for biomass conversion, J. Catal. 279 (2011) 257–268.
[26] S.P. Elangovan, V. Krishnasamy, V. Murugesan, Synthesis, characterization and catalytic activity of ZAPO-5 and ZAPO-11, Catal. Lett. 36 (1996) 271–277.
[27] W. Fang, A. Riisager, Efficient valorization of biomass-derived furfural to fuel bio-additive over aluminum phosphate, Appl. Catal. B: Environ. 298 (2021), 120575.
[28] T. Roisnel, J. Rodríguez-Carvajal, WinPLOTR: a windows tool for powder diffraction patterns analysis, Mater. Sci. Forum 378–381 (2001) 118–123.
[29] J. Rodríguez-Carvajal, Recent advances in magnetic structure determination by neutron powder diffraction, Phys. B: Condens. Matter 192 (1993) 55–69.
[30] J.T. Scanlon, D.E. Willis, Calculation of flame ionization detector relative response factors using the effective carbon number concept, J. Chromatogr. Sci. 23 (1985) 333–340.

[31] A. Jain, S.P. Ong, G. Hautier, W. Chen, W.D. Richards, S. Dacek, S. Cholia, D. Gunter, D. Skinner, G. Ceder, K.A. Persson, Commentary: the materials project: a materials genome approach to accelerating materials innovation, Appl. Mater. 1 (2013).
[32] G. Kresse, J. Furthmüller, Efficient iterative schemes for ab initio total-energy calculations using a plane-wave basis set, Phys. Rev. B 54 (1996) 11169.
[33] J.P. Perdew, K. Burke, M. Ernzerhof, Generalized gradient approximation made simple, Phys. Rev. Lett. 77 (1996) 3865–3868.
[34] J. Wellendorff, K.T. Lundgaard, A. Møgelhøj, V. Petzold, D.D. Landis, J.K. Nørskov, T. Bligaard, K.W. Jacobsen, Density functionals for surface science: exchange-correlation model development with Bayesian error estimation, Phys. Rev. B 85 (2012).
[35] A.J. Medford, J. Wellendorff, A. Vojvodic, F. Studt, F. Abild-Pedersen, K. W. Jacobsen, T. Bligaard, J.K. Nørskov, Assessing the reliability of calculated catalytic ammonia synthesis rates, Science 345 (2014) 197–200.
[36] J. Wellendorff, T.L. Silbaugh, D. Garcia-Pintos, J.K. Nørskov, T. Bligaard, F. Studt, C.T. Campbell, A benchmark database for adsorption bond energies to transition metal surfaces and comparison to selected DFT functionals, Surf. Sci. 640 (2015) 36–44.
[37] T.J. Goncalves, P.N. Plessow, F. Studt, On the accuracy of density functional theory in zeolite catalysis, ChemCatChem 11 (2019) 4368–4376.
[38] G. Kresse, D. Joubert, From ultrasoft pseudopotentials to the projector augmented-wave method, Phys. Rev. B 59 (1999) 1758–1775.
[39] B. Zibrowius, E. Löffler, M. Hunger, Multinuclear MAS n.m.r, and i.r. spectroscopic study of silicon incorporation into SAPO-5, SAPO-31, and SAPO-34 molecular sieves, Zeolites 12 (1992) 167–174.
[40] M.K. Dongare, D.P. Sabde, R.A. Shaikh, K.R. Kamble, S.G. Hegde, Synthesis, characterization and catalytic properties of ZrAPO-5, Catal. Today 49 (1999) 267–276.
[41] V.L. Sushkevich, I.I. Ivanova, S. Tolborg, E. Taarning, Meerwein–Ponndorf–Verley–Oppenauer reaction of crotonaldehyde with ethanol over Zr-containing catalysts, J. Catal. 316 (2014) 121–129.
[42] R. Shannon, Revised effective ionic radii and systematic studies of interatomic distances in halides and chalcogenides, Acta Cryst. A 32 (1976) 751–767.
[43] S.H. Jhung, Y.K. Hwang, J.-S. Chang, S.-E. Park, Effect of acidity and anions on synthesis of AFI molecular sieves in wide pH range of 3–10, Microporous Mesoporous Mater. 67 (2004) 151–157.
[44] H.P. Winoto, Z.A. Fikri, J.-M. Ha, Y.-K. Park, H. Lee, D.J. Suh, J. Jae, Heteropolyacid supported on Zr-Beta zeolite as an active catalyst for one-pot transformation of furfural to γ-valerolactone, Appl. Catal. B: Environ. 241 (2019) 588–597.
[45] B. Tang, W. Dai, X. Sun, G. Wu, N. Guan, M. Hunger, L. Li, Mesoporous Zr-Beta zeolites prepared by a post-synthetic strategy as a robust Lewis acid catalyst for the ring-opening aminolysis of epoxides, Green Chem. 17 (2015) 1744–1755.
[46] D.C. Liu, B.Q. Zhang, X.F. Liu, J. Li, Cyclohexane oxidation over AFI molecular sieves: effects of Cr, Co incorporation and crystal size, Catal. Sci. Technol. 5 (2015) 3394–3402.
[47] P.A. Barrett, G. Sankar, C.R.A. Catlow, J.M. Thomas, X-ray absorption spectroscopic study of Brønsted, Lewis, and redox centers in cobalt-substituted aluminum phosphate catalysts, J. Phys. Chem. 100 (1996) 8977–8985.
[48] G. Lischke, B. Parlitz, U. Lohse, E. Schreier, R. Fricke, Acidity and catalytic properties of MeAPO-5 molecular sieves, Appl. Catal. A: Gen. 166 (1998) 351–361.
[49] G. Muller, J. Bodis, G. EderMirth, J. Kornatowski, J.A. Lercher, In situ FT-IR microscopic investigation of metal substituted $AlPO_4$-5 single crystals, J. Mol. Struct. 410 (1997) 173–178.
[50] V.K. Nataša Novak Tušar, Silvano Geremia, Gilberto Vlaic, A zinc-rich CHA-type aluminophosphate, Zeolites 15 (1995) 708–713.
[51] M. Hartmann, L. Kevan, Substitution of transition metal ions into aluminophosphates and silicoaluminophosphates: characterization and relation to catalysis, Res. Chem. Intermed. 28 (2002) 625–695.
[52] M.J. Climent, A. Corma, V. Fornés, R. Guil-Lopez, S. Iborra, Aldol condensations on solid catalysts: A cooperative effect between weak acid and base sites, Adv. Synth. Catal. 344 (2002) 1090–1096.
[53] R. Zeidan, M. Davis, The effect of acid–base pairing on catalysis: An efficient acid–base functionalized catalyst for aldol condensation, J. Catal. 247 (2007) 379–382.
[54] N.C. Ellebracht, C.W. Jones, Optimized cellulose nanocrystal organocatalysts outperform silica-supported analogues: cooperativity, selectivity, and bifunctionality in acid-base aldol condensation reactions, ACS Catal. 9 (2019) 3266–3277.
[55] Q. Deng, J.S. Xu, P.J. Han, L. Pan, L. Wang, X.W. Zhang, J.J. Zou, Efficient synthesis of high-density aviation biofuel via solvent-free aldol condensation of cyclic ketones and furanic aldehydes, Fuel Process. Technol. 148 (2016) 361–366.
[56] R. Xing, A.V. Subrahmanyam, H. Olcay, W. Qi, G.P. van Walsum, H. Pendse, G. W. Huber, Production of jet and diesel fuel range alkanes from waste hemicellulose-derived aqueous solutions, Green Chem. 12 (2010) 1933–1946.
[57] J. Cueto, L. Faba, E. Diaz, S. Ordonez, Optimization of the process conditions for minimizing the deactivation in the furfural-cyclopentanone aldol condensation in a continuous reactor, Appl. Catal. B: Environ. 263 (2020), 118341.
[58] A. Bohre, M.I. Alam, K. Avasthi, F. Ruiz-Zepeda, B. Likozar, Low temperature transformation of lignocellulose derived bioinspired molecules to aviation fuel precursor over magnesium-lanthanum mixed oxide catalyst, Appl. Catal. B: Environ. 276 (2020), 119069.
[59] X. Meng, Y. Yang, L. Chen, M. Xu, X. Zhang, M. Wei, A control over hydrogenation selectivity of furfural via tuning exposed facet of Ni catalysts, ACS Catal. 9 (2019) 4226–4235.
[60] W. Liu, Y. Yang, L. Chen, E. Xu, J. Xu, S. Hong, X. Zhang, M. Wei, Atomically-ordered active sites in NiMo intermetallic compound toward low-pressure hydrodeoxygenation of furfural, Appl. Catal. B: Environ. 282 (2021), 119569.
[61] H. Ishikawa, M. Sheng, A. Nakata, K. Nakajima, S. Yamazoe, J. Yamasaki, S. Yamaguchi, T. Mizugaki, T. Mitsudome, Air-stable and reusable cobalt phosphide nanoalloy catalyst for selective hydrogenation of furfural derivatives, ACS Catal. 11 (2021) 750–757.
[62] R. Osuga, Y. Hiyoshi, T. Yokoi, J.N. Kondo, Reaction-probe infrared investigation on drastic change in reactivity of mesoporous silica for acetalization of cyclohexanone with methanol; pore-size dependence, Microporous Mesoporous Mater. 278 (2019) 91–98.
[63] Y. Chai, S. Liu, Z.-J. Zhao, J. Gong, W. Dai, G. Wu, N. Guan, L. Li, Selectivity modulation of encapsulated palladium nanoparticles by zeolite microenvironment for biomass catalytic upgrading, ACS Catal. 8 (2018) 8578–8589.
[64] M. Huang, S. Kaliaguine, A. Auroux, Lewis basic and Lewis acidic sites in zeolites, Stud. Surf. Sci. Catal. 97 (1995) 311–318.
[65] R.A. Schoonheydt, P. Geerlings, E.A. Pidko, R.A. van Santen, The framework basicity of zeolites, J. Mater. Chem. 22 (2012) 18705.